FORCED CONVECTION IN A SELF HEATING POROUS CHANNEL: LOCAL THERMAL NONEQUILIBIUM MODEL

by

Azzedine ABDEDOU [1,2*], Khedidja BOUHADEF [2] and Rachid BENNACER[3]

[1] Département du Génie Mécanique, Faculté de Génie de Construction, Université Mouloud Mammeri De Tizi Ouzou, Algérie
[2]USTHB – Faculty of Mechanical and Process Engineering (FGMGP)
Laboratory of Multiphase Transport and Porous Media (LTPMP) – Algeria
[3] LMT-ENS Cachan, 61 av. du president Wilson, F-94235 Cachan Cedex, France

[*] Corresponding author, Email: abdedou.azzedine@gmail.com

Laminar forced convection flow through a parallel plates channel completely filled with a saturated porous medium where occurs a uniform heat generation per unit volume with volumetric heat generation is investigated numerically. The Darcy-Brinkman model is used to describe the fluid flow. The energy transport mathematical model is based on the two equations model which assumes that there is no local thermal equilibrium ***(LTNE)*** *between the fluid and the solid phases. The dimensionless governing equations with the appropriate boundary conditions are solved by direct numerical simulation. The effect of the controlling parameters, Biot number, thermal conductivities ratio, heat generation rate and the Reynolds number on the LTE needed and sufficient condition is analysed. The results reveal essentially that the LTE condition is unfavourably affected by the increase in the heat generation rate, the thermal conductivities ratio and the decrease in the Biot number. In addition, for a given heat generation rate, the effect of Reynolds number on the LTE condition is reversed depending on the conductivities ratio threshold.*

Keywords: *Forced convection, porous media, Local thermal non equilibrium, heat generation.*

1. Introduction

Convective heat transfer in fluid-saturated porous media have received much attention for the last decades. Indeed, the theme is wild and presents currently still much interest. It is due to its relevance in a wide range of application in many applications, such as thermal insulation, catalytic and chemical particle beds, transpiration cooling, geothermal energy system heat exchanger, packed bed regenerators, solid matrix heat exchangers and nuclear waste disposal etc, etc.

Most of the investigations assume local thermal equilibrium between the fluid and the solid phases at any location in the porous medium [1-3]. This assumption is inappropriate for a number of cases such

as heat energy storage systems and nuclear reactor modeling where the temperature difference between the fluid and the solid phase becomes crucial; therefore the local thermal non equilibrium model (LTNE) must be used. Analytical study, Brinkman-Darcy model, for fully developed forced convective heat transfer in a tube partially filled with metallic foam with interfacial coupling conditions for the LTNE model was conducted by Xu *et al* [4]. Such kind of flow with multiple discrete heated sources in a horizontal channel containing metal-foam was investigated numerically in order to enhance the heat transfer by Chen et al [5]. The used Darcy–Brinkman–Forchheimer flow model and LTNE allowed a better understanding of the situations under which the local thermal equilibrium (LTE) assumption would be justifiable. The authors have also found that the specific choices in certain governing parameters, such as the permeability, pore density, fiber diameter and the effective thermal conductivity of the metal-foam porous layer, can have profound effects on the heat sources cooling. Phanikumar and Mahajan [6] have examined numerically and experimentally the flow and heat transfer characteristics in metal foam samples heated from below, by using a two-equation model for the temperature and by integrating the porous media and the clear fluid domains using the single-domain approach. They found that the temperature predictions based on the LTNE are in better agreement with the experimental data compared to those based on the LTE model. Another numerical study in natural convection, conducted by Pippal and Bera [7] reported the temperature difference, using LTNE, between solid porous matrix and saturated fluid in an enclosure. They found that for a given thermal conductivities ratio, when the interstitial heat transfer coefficient value is relatively high, the temperature contours of two phases becomes almost identical in magnitude as well as patterns point of view, which indicates that equilibrium state between two phases is achieved.

Other studies have been conducted in order to define more accurately the circumstances in which the condition of the local thermal equilibrium or non-equilibrium is verified, which allowed defining a multitude of criteria to better optimize the evaluation of heat exchanges. Thus, Lee and Vafai [8] employed the thermal non equilibrium model to investigate the forced convective flow through a channel filled with a porous medium. They obtained analytical solutions for the fluid and solid phase temperature distributions and the heat transfer characteristics were classified into three regimes, and the study established conditions for which one-equation model is valid. Khashan and AL-Nimr [9] have performed a numerical study to examine the validity of the local thermal equilibrium LTE assumption for forced convective heat transfer of non-Newtonian fluids in a channel confined by two horizontal plane plates. The results obtained over broad ranges of representative dimensionless parameters are used to map conditions for which the local thermal equilibrium assumption can or cannot be employed. Quantitative LTE validity maps that reflect the proportional effect of each parameter as related to others are presented. Marafei and Vafai [10] obtained analytical expressions for the fluid and solid phases temperatures distributions for convective flow through a channel with a constant heat flux applied at walls and accounting for both boundary and inertial effects. Moreover Jaballah et al [11] have studied numerically the mixed convection in a channel with porous layers using the thermal non equilibrium model. They clearly showed the limits of the interstitial heat transfer coefficient and thermal conductivity ratio parameters over which the two models LTE and LTNE of the two phases fluid and solid will be identical.

The purpose of the present work is to examine the forced convective heat transfer in a plane channel filled with a saturated porous medium in which occurs an internal heat generation in the solid phase.

The main objective is to study the temperature difference profile evolution between the fluid and the solid phases, as function of the transverse position for different channel sections by moving from the inlet to the outlet. It will also address the validity of the local thermal equilibrium (LTE) assumption in the flow and the porous medium. The LTE condition is tested for various values of dimensionless parameters such as interstitial Biot number, thermal conductivity ratio, flow Reynolds number based on the mean value of the velocity in the channel section and heat generation rate per unit volume, occurring in the porous medium.

2. Problem statement and governing equations

2.1. Physical domain

The considered physical model is shown in fig. 1 with used coordinates. The system under investigation is a horizontal parallel-plate channel completely filled with a saturated porous medium having a constant porosity. It is assumed that the fluid is incompressible and the flow is laminar (what is possible when the Reynolds number based on the particle diameter, $Re_p<100$ [12]), in steady state and two-dimensional. The fluid enters the channel with a uniform velocity and temperature distributions, U_{in} and T_{in}, respectively. The horizontal surfaces are supposed to be at constant temperature (T_w) higher than the inlet fluid temperature.

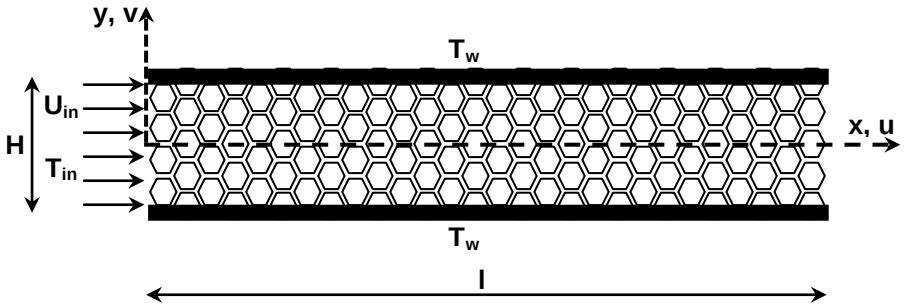

Figure 1. Schematic representation of the considered porous channel

2.2. Governing equations

To write the governing equations, following assumptions are made as:

- The thermophysical properties of the fluid and porous media are assumed to be constant.
- Natural convection and radiative heat transfer are neglected according to other modes of heat transfer.
- There is no fluid phase change in the medium.
- The convective fluid and the porous solid are not in local thermodynamic equilibrium (two energy equations model).
- The solid porous matrix (porous media) is with uniform volumetric heat generation.
- The dynamic flow is described by the Brinkman extended Darcy model which permits to combine the Darcy flow with the Stokes flow in order to extend the Stokes drag force on a particle to include the effects of the neighbouring particles [13].

Under above assumptions, the continuity, momentum and energy equations can be written in dimensionless form as follow:

$$\frac{\partial U}{\partial X}+\frac{\partial V}{\partial Y}=0 \tag{1}$$

$$U\frac{\partial U}{\partial X}+V\frac{\partial U}{\partial Y}=-\frac{\partial P}{\partial X}+\frac{1}{Re}\left(\frac{\partial^2 U}{\partial X^2}+\frac{\partial^2 U}{\partial Y^2}\right)-\frac{1}{ReDa}U \tag{2}$$

$$U\frac{\partial V}{\partial X}+V\frac{\partial V}{\partial Y}=-\frac{\partial P}{\partial Y}+\frac{1}{Re}\left(\frac{\partial^2 V}{\partial X^2}+\frac{\partial^2 V}{\partial Y^2}\right)-\frac{1}{ReDa}V \tag{3}$$

$$U\frac{\partial \theta_f}{\partial X}+V\frac{\partial \theta_f}{\partial Y}=\frac{1}{PrRe}\left(\frac{\partial^2 \theta_f}{\partial X^2}+\frac{\partial^2 \theta_f}{\partial Y^2}\right)+6\frac{(1-\varepsilon)}{\varepsilon}\frac{Bi}{PrRe_p}\left(\theta_s-\theta_f\right) \tag{4}$$

$$\frac{\partial^2 \theta_s}{\partial X^2}+\frac{\partial^2 \theta_s}{\partial Y^2}-6\frac{Bi}{R_k}\frac{Re}{Re_p}\left(\theta_s-\theta_f\right)+\frac{R_q}{R_k}=0 \tag{5}$$

Where the following dimensionless variables have been used:

$$X=\frac{x}{H},\quad Y=\frac{y}{H},\quad U=\frac{u}{U_{in}},\quad V=\frac{v}{U_{in}},\quad P=\frac{\varepsilon^2 p}{\rho_f U_{in}^2},\quad L=\frac{\ell}{H},\quad \theta=\frac{T-T_{in}}{T_w-T_{in}} \tag{6}$$

Equations (1)-(5) contain the Reynolds number Re, the Darcy number Da, the Prandtl number Pr, the local Biot number Bi, the thermal conductivity ratio R_k and the dimensionless heat flux ratio, which are respectively defined as:

$$Re=\frac{\rho_f U_{in} H}{\varepsilon\mu},\quad Da=\frac{K}{\varepsilon H^2},\quad Pr=\frac{\varepsilon\nu_f}{\alpha_f},\quad Bi=\frac{h_{sf}H}{k_f},\quad R_k=\frac{k_s}{k_f},\quad R_q=\frac{q}{q_{ref}} \tag{7}$$

It should be noted that the dimensionless form of the energy equations is obtained, among other things, considering the expression of specific surface area given by the correlation of Wakaoo et al [14] based on the porosity ε and the particle diameter d_p of the porous medium, as:

$$a_{sf}=6\frac{(1-\varepsilon)}{d_p} \tag{8}$$

2.3. Boundary conditions

The flow and heat transfer characteristics are symmetrical around X -axis as shown in fig. 1. Hence, only one half is considered to be the computational domain. Based on this, the appropriate boundary conditions can be mathematically expressed as follows:

$$U(0,Y)=1,\ V(0,Y)=\theta_s(0,Y)=\theta_f(0,Y)=0 \tag{9}$$

$$U\left(X,\frac{H}{2}\right)=V\left(X,\frac{H}{2}\right)=0,\ \theta_s\left(X,\frac{H}{2}\right)=\theta_f\left(X,\frac{H}{2}\right)=1 \tag{10}$$

$$\frac{\partial U(X,0)}{\partial Y}=\frac{\partial V(X,0)}{\partial Y}=\frac{\partial \theta_f(X,0)}{\partial Y}=\frac{\partial \theta_s(X,0)}{\partial Y}=0 \tag{11}$$

$$\frac{\partial U(L,Y)}{\partial X}=\frac{\partial V(L,Y)}{\partial X}=\frac{\partial \theta_f(L,Y)}{\partial X}=\frac{\partial \theta_s(L,Y)}{\partial X}=0 \tag{12}$$

3. Numerical procedure

3.1. Numerical method

The numerical computation was carried out with the control volume approach [15], using rectangular cells with constant mesh spacing in both directions (axial and transverse). The first order upwind scheme is applied for the convection–diffusion formulation in eqs. (1)-(4). The central differencing scheme is used for the diffusion terms (energy and momentum equations). Staggered grids and SIMPLE algorithm as suggested by Patankar [15] are adopted to treat the coupling between velocity

and pressure fields. The set of obtained algebraic equations are solved using a numerical algorithm based on an iterative Strongly Implicit Procedure developed by Stone [16]. The iteration process is terminated if the following condition is satisfied:

$$max\left|\frac{\Phi_{i,j}^{m+1}-\Phi_{i,j}^{m}}{\Phi_{i,j}^{m}}\right| \leq 10^{-7} \quad (13)$$

Where Φ represents a dependent variable U, V, P, θ_f and θ_s. The subscripts i, j indicate the grid point and uperscript m denotes the iteration number. Relaxation factors are employed to avoid divergence during the iteration.

The iterative computation process starts with the estimation of the pressure field, and then the momentum equations are solved to compute the velocity components. The obtained correction pressure equation is solved and then the velocity components and pressure are corrected with the new values. The process is repeated until convergence. With this condition, the two temperature equations for the both fluid and solid phases are solved until reach satisfactory convergence during the iterative process. After convergence, the difference between temperatures of the two phases is evaluated in each point of the computational domain.

3.2. Grid independence study

Concerning the mesh refinement or grid size effect on the numerical solution, various grid systems from 200 x 110 to 350 x 140 (in X- and Y- directions, respectively) are tested to compare the average Nusselt numbers values for each phase. The results are presented in tab. 1 for various values of *Bi* and R_k at fixed *Re* = 100, *Da* = 10^{-4} and R_q= 0. The maximum discrepancy in the values of $\overline{Nu_f}$ or $\overline{Nu_s}$ between the grid 250 x120 and the finest one (350 x 140) for all values of *Bi* and R_k is less than 2.63 %. Thus, the mesh size (250 x 120) is considered good enough to generate grid independence results.

Table 1. Comparison of the results for different *Bi* and R_k values with *Re*=100, *Da*=10^{-4}, R_q=0, ε=0.9, Re_p=1 and *Pr*=0.7

Bi	R_k	200 x 110		250 x 120		300 x 130		350 x 140	
		$\overline{Nu_s}$	$\overline{Nu_f}$	$\overline{Nu_s}$	$\overline{Nu_f}$	$\overline{Nu_s}$	$\overline{Nu_f}$	$\overline{Nu_s}$	$\overline{Nu_f}$
1	1	2.592	2.816	2.614	2.831	2.640	2.851	2.669	2.876
Error (%)		2.88	2.08	2.06	1.56	1.08	0.86	-	-
10	1	2.728	2.807	2.747	2.823	2.771	2.844	2.798	2.869
Error (%)		2.50	2.16	1.82	1.60	0.96	0.87	-	-
100	10	2.315	2.375	2.328	2.387	2.355	2.412	2.391	2.446
Error (%)		3.17	2.90	2.63	2.41	1.50	1.39	-	-

3.3. Code validation

To check the present numerical simulation which is implemented in a Fortran program, comparison is made with the previously published analytical results obtained by Hooman and Guergenci [17], for the case of the forced convection in a channel at constant walls temperatures and with viscous dissipation effects. The exact solution of the asymptotic Nusselt number given by in the cited work [17] is:

$$Nu = \frac{S^2\left(\frac{(3-C_1-C_2)}{\sigma}+(C_1+C_2-1)tanh^2S\right)}{\left(1+\frac{1-C_1-C_2}{2cosh^2S}\right)\left(\frac{\sigma S^2}{3}-1\right)+(2-C_1)\frac{(-3+\sigma tanh^2S)}{2}+(1-C_1-C_2)\frac{\left((4-\sigma)tanh^2S+3\right)}{24}} \quad (14)$$

With: $$S = Da^{-\frac{1}{2}} \text{ and } \sigma = \left(1-\frac{tanh(S)}{S}\right)^{-1} \quad (15)$$

The values of the coefficients C_1, C_2 and C_3 define which model of the dimensionless viscous dissipation function used in the energy equation, as detailed by Hooman and Guergenci [17]:

Model 1 for the Darcy model ($C_1 = 0$ and $C_2 = 0$), model 2 for the power of drag force model ($C_1 = 1$ and $C_2 = 0$) and model 3 for the clear fluid compatible model ($C_1 = 0$ and $C_2 = 1$).

Figure 2 shows a good agreement between the numerical approach and the analytical results given by eq. (14) for the models 1 & 2 for all values of S. The maximum discrepancy between the two results appears for the model 3 for a small range of S values and does not exceed 1.6 %, what is sufficiently acceptable.

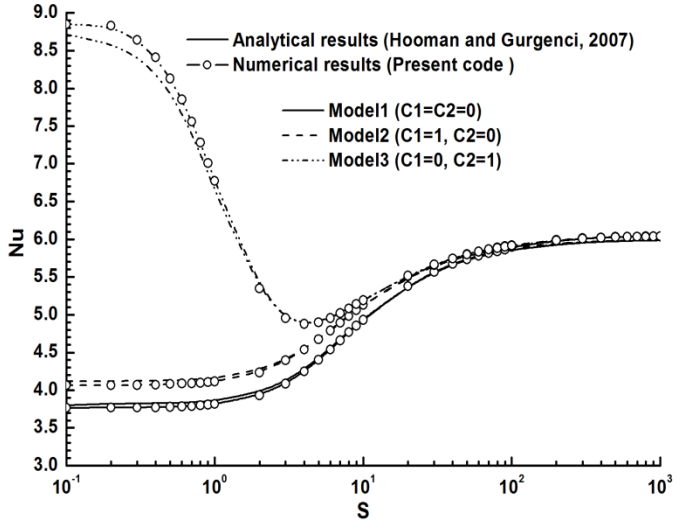

Figure 2. Comparison of asymptotic Nusselt number profile versus S with that of [17]

4. Results and discussion

Computations were conducted with some fixed controlling parameter: the Prandtl number is assumed to be that of the air (*Pr*=0.7, value frequently assumed in the literature [11]), the porosity of the porous medium (ε=0.9), the channel aspect ratio (*L*=10), the particle Reynolds number (Re_p=1) and the Darcy number (Da=10^{-4}). Several criteria have been admitted in the literature to define the local thermal equilibrium condition (**LTE**) [8-11]. The criterion adopted in this study is based on the absolute difference in local temperatures of the fluid and solid phases at each point of the computational domain [9], which is traduced mathematically as:

$$\Delta\theta_{i,j} = \left|\theta_{s_{i,j}} - \theta_{f_{i,j}}\right| \quad (16)$$

It has been well accepted that the condition of local thermal equilibrium (**LTE**) holds if $\Delta\theta_{i,j} \leq 5\%$ and inversely, the local thermal non equilibrium (**LTNE**) becomes pronounced if $\Delta\theta_{i,j} > 5\%$.

The objective of this criterion is to show the spatial distribution of the local thermal non equilibrium (or equilibrium) over the channel length. So from this test one can delineate the channel areas where there is local thermal equilibrium and the areas where there is local thermal non equilibrium in the (X, Y) plan. The maximum value of the absolute local temperature difference between the fluid and solid phases in the entire channel can serve as another criterion to determine the **LTE** and **LTNE** areas in the (*Bi*, R_k) plan. These **LTE** and **LTNE** zones in the (*Bi*, R_k) chart are mathematically defined by the conditions max ($\Delta\theta_{i,j}$) ≤ 5% and max ($\Delta\theta_{i,j}$) > 5%, respectively. The results are presented and discussed in terms of the fluid and solid temperatures difference and **LTE** validity maps. In the first part of the results, the plots show the temperature difference profiles evolution between the fluid and the solid phases over the channel length from the inlet to the outlet. The second part of the results reported in this work concerns the effect of governing parameters such as the heat generation rate and the Reynolds number on the **LTE** validity map in the (*Bi*, R_k) plan.

4.1. Temperature difference profile

Figure 3 displays the absolute temperatures difference distribution between the solid and the fluid phases, as mentioned by eq. (16), as function of transverse coordinate for different axial positions over the channel length with a low Biot number value (*Bi*=0.01) for different solid-to-fluid thermal conductivity ratio values R_k. As shown in this figure, the difference between the temperatures of the two phases is highly enhanced from zero value, due to the imposed condition of local thermal equilibrium at the wall, towards the channel center value. It appears, also, that the temperature difference between the two phases is the largest in the inlet region, decreasing gradually with the evolution downstream. In fact, one can easily notice that, in the considered case (high heat generation in the solid phase) the local thermal non equilibrium is strongly pronounced in any point with maximum values on the central axis of the channel.

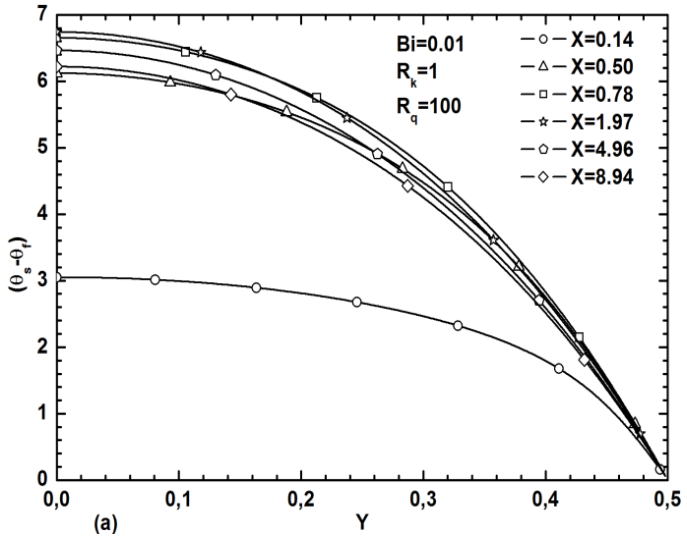

Figure 3. Temperature difference profile as a function of transverse distance at different axial positions for *Re*=100, *Da*=10^{-4} , *Rq*=100, *Bi*= 0.01 and R_k=1

When Biot number and thermal conductivities ratio take high values (*Bi*=10, R_k=100), it is observed from fig.4 that temperature difference between the two phases at the channel inlet becomes relatively important and gradually decreases to become constant and almost negligible by moving downstream of the channel. Here again, we see that the condition of local thermal equilibrium is strongly checked

on the whole channel except at the inlet region. This can mean that a significant increase in the conductivity of the solid allows a part of the generated heat to be evacuated by conduction in the solid and another part is evacuated by internal transfer to the fluid (high *Bi*) and then by convection towards outside.

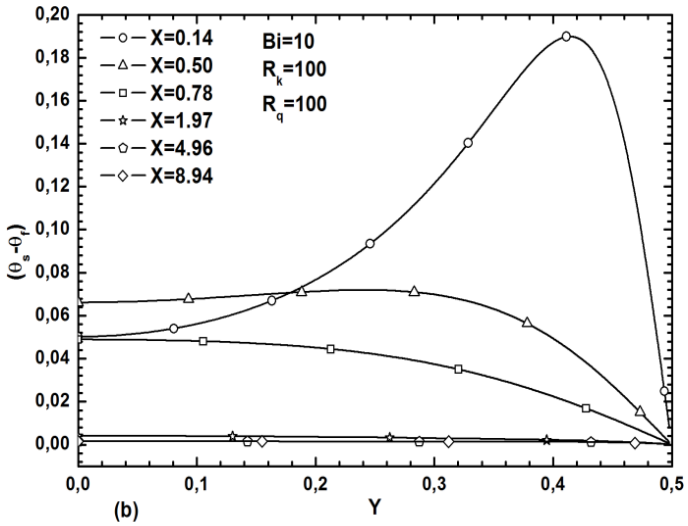

Figure 4. Temperature difference profile as a function of transverse distance at different axial positions for $Da=10^{-4}$, $Bi=10$ and $Re=R_k=Rq=100$

4.2. LTE validity maps

The following figures (5-7) represent maps delineating the validity areas of the local thermal equilibrium condition as function of Biot number (*Bi*) and thermal conductivities ratio (R_k), for a various controlling parameters such as the heat generation rate and the Reynolds number. As mentioned earlier, the boundary line separating the **LTE** and **LTNE** zones in the (*Bi*, R_k) chart is obtained when the condition max ($\Delta\theta_{i,j}$) $\leq$ 5% is satisfied in the entire channel under study. The mapping of the **LTE-LTNE** regions is performed using an inner Bi loop inside an outer R_k loop. For each selected R_q and/or *Re* value, and for each value of outer R_k loop, the inner *Bi* loop turns with an appropriate increment until the **LTE** condition is satisfied. The corresponding (*Bi*, R_k) values are saved and the process is repeating for the following incremented value of the outer R_k loop, but by starting the inner *Bi* loop from the previously stored value and so on. Therefore, the **LTE** area in the (*Bi*, R_k) plan is delimited by a succession of minimum Biot number (Bi_{min}) and maximum thermal conductivity ratio (R_{kmax}), defining so the boundary line between the **LTE** and **LTNE** areas.

Figure 5 shows the effect of heat generation rate in the solid phase on the **LTE** area for Reynolds number values of 25 and 100. The increase in heat generation reduces the **LTE** area much more for low values of *Bi* and R_k and low Reynolds number. This effect diminishes gradually as *Bi* and R_k increase, which is clearly illustrated by the convergence of boundary lines delimiting the **LTE-LTNE** regions for all considered heat generation rates. The *Bi* and R_k, values from which heat generation influence on the **LTE** condition becomes insignificant, depend on the Reynolds number. Thus, as shown in figure 5, for weak R_k values and in the absence of heat generation, the minimum *Bi* value required to satisfy the **LTE** condition for $Re = 25$ is Bi_1. For the same R_k value with the presence of heat generation, the solid phase temperature increases, due to the relatively low thermal conductivity

of the solid compared to that of the fluid, this causes the increasing in the temperature difference between the two phases and consequently reducing the **LTE** area. Under these circumstances, the **LTE** condition can be satisfied again by augmenting the interstitial heat exchange (increasing *Bi*) to evacuate the generated heat. Thus, the new minimum values of *Bi* on the **LTE-LTNE** boundary line are Bi_2 and Bi_3 for Rq = 50, and Rq = 100, respectively with $Bi_1 < Bi_2 < Bi_3$. Increasing R_k leads to the enhancement of the solid phase capacity to evacuate the heat generated by conduction and allows reducing significantly the difference of the temperatures between the two phases. The growth in heat generation is offset by the solid thermal conductivity rise, which explains the decrease of heat generation effect on the **LTE** area for high R_k values.

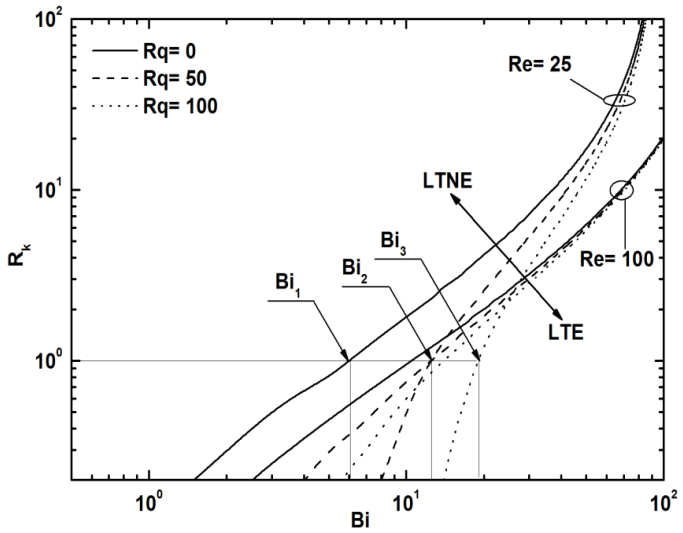

Figure 5. Effect of the heat generation rate on the R_k-*Bi* LTE validity map at *Re*=25 and *Re*=100

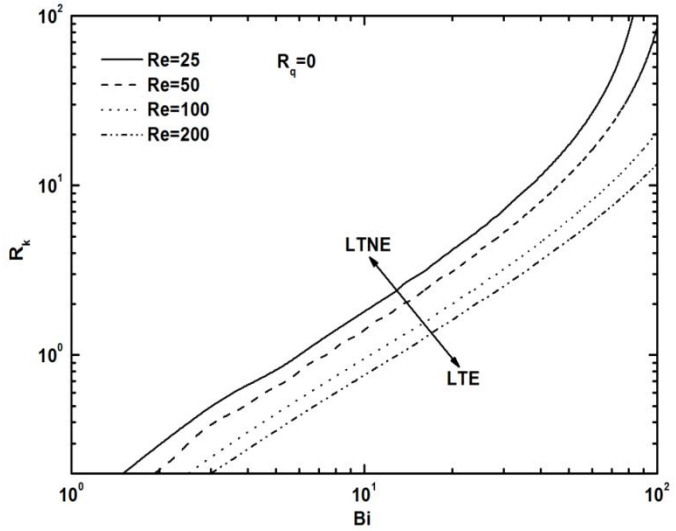

Figure 6. Effect of the Reynolds number on the R_k-*Bi* LTE validity map at *Rq*=0

Figure 6 shows the influence of the Biot number, the thermal conductivities ratio and the Reynolds number on the **LTE** condition for the case without heat generation in the solid phase. For each constant *Re* line, the area in the *Bi*-R_k plan mapped the right (down) represents the **LTE** area and those mapped to the left (above) represents the **LTNE** area. It is clear from this figure that for a constant *Re* and low R_k, the local thermal equilibrium is reached for low *Bi* values. As R_k increases, the minimum

required value of *Bi* to verify the **LTE** condition augments. The **LTE** condition is verified when the ratio of *Bi* and R_k takes a high value in the *Bi*-R_k plan ($\mathrm{Bi}/\mathrm{R_k} \gg 1$). Increasing *Re* number, which corresponds to augment the flow intensity, has an unfavorable effect on the **LTE** condition, by expanding the **LTNE** region in the *Bi*-R_k plan. It is clear from the energy equation of the fluid phase that augmenting the Reynolds number leads to the reduction of the conduction effects and the enhancement of the convection effect, causing the deepening of the temperature difference between the two phases. The high flow intensity doesn't allow a sufficient interstitial thermal communication.

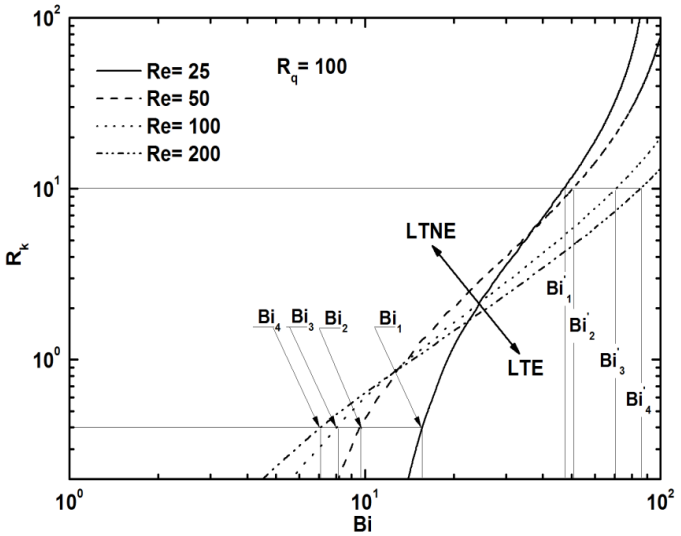

Figure 7. Effect of the Reynolds number on the R_k-*Bi* LTE validity map at *Rq*=100

The effect of the Reynolds number on the **LTE** condition with the presence of the heat generation in the solid phase strongly depends on the R_k values. As it is shown on fig. 7, the minimum required values of *Bi* from which the **LTE** condition is verified for different constant *Re* values (*Re*=25, 50, 100, 200) are Bi_1, Bi_2, Bi_3 and Bi_4, respectively, for a given low R_k value and Bi'_1, Bi'_2, Bi'_3 and Bi'_4, respectively, for a given high R_k value. It is clear from this figure that $Bi_1 > Bi_2 > Bi_3 > Bi_4$ and $\mathrm{Bi}'_1 < Bi'_2 < Bi'_3 < Bi'_4$. Thus the Reynolds number effect on the **LTE** condition is reversed depending on the R_k values. For a low R_k, augmenting *Re* leads to the increase of the **LTE** area. This effect is completely reversed when R_k reaches high values, by reducing the **LTE** region in the *Bi*-R_k plan. The Low R_k values leads to a significant solid temperature rise due to the low thermal conductivity of solid phase which traps the generated heat. When the Reynolds number rises the convective exchange between the wall and the fluid phase is enhanced, which thereby results in an increase of fluid temperature and thus reduces the gap with the solid phase temperature. When R_k takes high values, the solid phase capacity to remove the generated heat is significant. This triggers a downward trend in the temperature of the solid. Under these conditions rising the Reynolds number leads to the increase of the fluid temperature due to the high rate of the convective exchanges with the wall, which is in the opposite direction of the evolution of the solid temperature evolution and therefore results on the increase in the temperature gap between the two phases. As confirmed by the energy equation for the solid phase, the interaction between the Reynolds number and the heat generation rate closely depends on the diffusive term intensity, which is negligible for low R_k values and predominant for high R_k, ratios which explains the reversal effect of *Re* on the **LTE** condition. It is clear that the presence of the heat generation in the solid phase changes closely the LTE-LTNE border line trend which evolves from the linear tendency for the case without heat generation to the

asymptotic trends for two limit cases of low R_k values (thermal fluid dominant regime) and high R_k values (thermal solid dominant regime) as the heat generation increases, more significantly for low Reynolds numbers.

5. Conclusion

Forced convection in horizontal parallel plates channel completely filled with a saturated porous medium with internal heat generation in the solid phase has been numerically investigated. We have considered cases where local thermal non-equilibrium exists between the solid and the fluid phases as modeled by an inter-phase heat transfer coefficient. The dynamic field is described by the Brinkman extended Darcy model. It can be concluded from the results analysis that:

- The temperature difference value which can significantly increase in the inlet region of the channel will diminish when going downstream.
- The local thermal equilibrium is perfectly realized over the entire length of the channel when the interstitial exchange (*Bi*) is high and the thermal conductivity ratio (R_k) is low.
- The **LTE** condition is strongly affected by the dimensionless governing parameters. Therefore, the increase in the heat generation rate (R_q) has an unfavorable effect on the **LTE** condition. For the case without heat generation, the increase in the Reynolds number leads to reducing the **LTE** area in the *Bi*-R_k plan. When the heat generation becomes important, the increase in the Reynolds number has a favorable effect on the LTE condition for weak R_k values and an unfavorable effect on the **LTE** condition for high R_k values.
- At last, the **LTE** condition is very well verified for high Biot number values and low thermal conductivities ratio values, in other terms, when the rate between *Bi* and R_k takes high values ($Bi/R_k \gg 1$), independently on the operating conditions.
- Finally it should be noticed that all these results were obtained under the assumption of constant interstitial exchange coefficient and any eventual non homogeneity can lead to an amplification of the local thermal non equilibrium condition between the two phases.

Acknowledgment

Authors thank the Project PHC-Maghreb 3025TE (University of Lorraine/ENS Cachan) for supporting the present exchange

Nomenclature

a_{sf}	Specific surface area, [m^2m^{-3}]
Bi	Interstitial Biot number (=$h_{sf}H/k_f$), [-]
Da	Darcy number (=$K/\varepsilon H^2$), [-]
d_p	Pore diameter, [m]
h_{sf}	Interstitial heat transfer coefficient, [$Wm^{-2}K^{-1}$]
L	Dimensionless channel length (=l/H), [-]
P	Dimensionless pressure
Pr	Prandtl number (=$\varepsilon\nu/k_f$), [-]
q	Volumetric heat generation flux [Wm^{-3}]
q_{ref}	Reference heat flux $(T_w\text{-}T_{in})k_f/H^2$
Re	Reynolds number (=$\rho u_{in}H/\varepsilon\mu$), [-]
Re_p	Pore Reynolds number (=$Re_d/\varepsilon H$), [-]
u,v	velocity components [ms^{-1}]
U, V	Dimensionless velocity components
X	Dimensionless axial coordinate (= *x/H*), [-]
Y	Dimensionless transverse coordinate(= *y/H*),

Greek symbols

α_f	Thermal diffusivity $(k/\rho c)_f$
θ	Temperature,(= $(T\text{-}T_{in})/(T_w\text{-}T_{in})$), [-]
ε	Porosity

Subscripts

in	inlet
f	fluid
p	Pore

R_k	Thermal conductivity ratio (= k_s/k_f), [-]	ref	reference value
R_q	Dimensionless heat flux ratio (=q/q_{ref}), [-]	s	solid
T	Intrinsic fluid or solid temperature [K]	w	wall

References

[1] Ganji, D. D., Sajjadi. H., New analytical solution for natural convection of Darcian fluid in porous media prescribed surface heat flux, *Thermal sciences., 15* suppl. 2 (2011), pp. S221-S227.

[2] Chauhan, D. S. and V, Kumar., Heat transfer effects in a couette flow through a composite channel partly filled by a porous medium with a transverse sinusoidal injection velocity and heat source, *Thermal Sciences., 15* suppl. 2 (2011), pp. S175-S186.

[3] Younsi. R., Computational analysis of MHD flow, heat and mass transfer in trapezoidal porous cavity, *Thermal Sciences., 15* (2009), N°1, pp. 13-22.

[4] Xu, J., Qu, Z. G., Tao, W. Q., Analytical solution of forced convective heat transfer in tubes partially filled with metallic foam using the two-equation model, *Int. J. Heat Mass Transfer., 54* (2011), pp. 3846-3855.

[5] Chen, C. C., Huang, P. C., Hwang, H. Y., Enhanced forced convective cooling of heat sources by metal-foam porous layers, *Int. J. Heat Mass Transfer., 58* (2013), pp. 356-373.

[6] Phanikumar, M. S., Mahajan, R.L., Non-Darcy natural convection in high porosity metal foams, *Int. J. Heat Mass Transfer., 45* (2002), pp. 3781–3793.

[7] Pippal, S., Bera, P., A thermal non-equilibrium approach for 2D natural convection due to lateral heat flux: Square as well as slender enclosure, *Int. J. Heat Mass Transfer., 56* (2013), pp.501–515.

[8] Lee, D.Y., Vafai, K., Analytical characterization and conceptual assessment of solid and fluid temperature differentials in porous media, *Int. J. Heat Mass Transfer., 42*(1999), pp. 423-435.

[9] Khashan, S. A., AL-Nimr, M. A., Validation of the local thermal equilibrium assumption in forced convection of non-Newtonian fluids through porous channels, *Transport in Porous Media., 61* (2005), pp. 291–305.

[10] Marafie, A., Vafai, K., Analysis of non-darcian effects on temperature differentials in porous media, *Int. J Heat Mass Transfer., 44* (2001), pp. 4401-4411.

[11] Jaballah, S., Sammouda, H., Bennacer, R., Study of the mixed convection in a channel with porous layers using a thermal nonequilibrium model, *J. Porous Media.*, 15.1 (2012), pp. 51-62.

[12] Nield, D. A., Bejan, A., *Convection in porous media*, Springer-Verlag., 3rd Edition New York, 2006.

[13] Kaviany, M., *Principles of heat transfer in porous media*, Springer-Verlag, 2nd edition corrected., New York, 1999.

[14] Wakaoo, N., Kaguei, S., Funazkri, T., Effect of fluid dispersion coefficients on particle to fluid heat transfer coefficients in packed beds, Chem. Engng Sci., *34* (1979), pp. 325-336.

[15] Patankar, S. V., Numerical heat transfer and fluid flow, Hemisphere, New York (1980).

[16] Stone, H.L., Iterative solution of implicit approximations of multidimensional partial differential equations, *SIAM J. Num. Anal., 5* (1968), N°. 3.

[17] Hooman, B., Guergenci, H., Effects of viscous dissipation and boundary conditions on forced convection in a channel occupied by a saturated porous medium, *Transp. Porous Med., 68* (2007), pp. 301-319.